

Article

An Efficient Structural Optimization Method for the Hinge Beam of a Cubic Press

Jin Shang, Xuan Sun *, Ting Liu and Jiguang Jia

School of Mechanic and Control Engineering, Guilin University of Technology, Guilin 541000, China; sjglut@163.com (J.S.); 2120211165@glut.edu.cn (T.L.); j1042958076@163.com (J.J.)

* Correspondence: sunxuan@glut.edu.cn

Abstract: This study proposes a novel approach to optimize the structure of the hinge beam in cubic presses, aiming to enhance the safety and reduce costs. The finite element method is used to analyze the stress distribution of the hinge beam under operating conditions, revealing a significant stress concentration at the oil inlet edge. To optimize the structure, the Taguchi method, the NSGA-II multi-objective optimization algorithm, and the entropy-TOPSIS method are combined to consider both the maximum stress and total weight. The results demonstrate a reduction of 199.121 kg and 11.97 MPa in the total weight and maximum stress of the hinge beam, respectively, representing a decrease of 4.12% and 1.72%. Furthermore, the simulation results of the optimal structure demonstrate a high degree of accuracy, with only 0.27% difference between the algorithm-optimized and simulation values. The proposed optimization method not only improves the efficiency of the optimization, but also avoids the mutual exclusion between the maximum stress and total weight. It significantly improves the reliability of the hinge beam and reduces its manufacturing costs, thereby shortening the development cycle of the new hinge beam.

Keywords: cubic press; hinge beam; maximum stress; total weight; multi-objective optimization



Citation: Shang, J.; Sun, X.; Liu, T.; Jia, J. An Efficient Structural Optimization Method for the Hinge Beam of a Cubic Press. *Machines* **2023**, *11*, 503. <https://doi.org/10.3390/machines11050503>

Academic Editor: Zheng Chen

Received: 27 March 2023

Revised: 16 April 2023

Accepted: 19 April 2023

Published: 22 April 2023



Copyright: © 2023 by the authors. Licensee MDPI, Basel, Switzerland. This article is an open access article distributed under the terms and conditions of the Creative Commons Attribution (CC BY) license (<https://creativecommons.org/licenses/by/4.0/>).

1. Introduction

Diamond is the hardest, strongest, and most wear-resistant material found in nature, and it is widely used in aerospace, geological drilling, medical and military defense [1–5]. The high price and low production limits of natural diamonds require synthetic diamonds to meet the industry’s great demand [6,7]. Diamonds are synthesized by reacting carbonaceous raw materials such as graphite with certain metals through ultra-high pressure and high-temperature techniques [8].

With low material consumption, low processing and maintenance costs, fast boosting and bucking, and high production efficiency, the cubic press is the key equipment for synthesizing diamonds and has an irreplaceable role [9]. In the process of synthesizing the diamond using the cubic press, the hinge beam undergoes three stages of pressurization, pressure-holding, and decompression and is subjected to alternating cyclic loads for a long time, leading to fatigue fracture [10]. Moreover, under rated operating conditions, the bottom and ears of hinge beam are under great pressure, which is prone to bottom fracture and ear fracture.

At the same time, a hinge beam can weigh more than 4 tons, accounting for a significant portion of the machine’s cost. Therefore, understanding how to reasonably design the hinge beam structure, improve its fatigue strength, and achieve lightweight is the key to developing a new generation of hinge beams. In traditional design, parts are often conservatively designed with a high safety factor to prevent accidental risk or premature fatigue damage [11], which significantly increases the weight and manufacturing cost of the hinge beam.

With the development of computer technology, finite element simulation has been widely used in industry. It provides techniques for verification of strength and structural

optimization of parts [12,13], which extends the service life of parts, shortens the development cycle, and reduces costs. Ma [14] investigated the internal stress distribution of the hinge beam using the finite element method and analyzed the fracture of the hinge beam ears due to fatigue and overload. The simulation results found that the internal stress distribution of the hinge beam is not uniform, there is stress concentration, and the maximum stress is located at the outside of hinge beam ear. However, the reasons why the stress concentration at the outside of hinge beam ear were not analyzed, and no corresponding optimization scheme was proposed.

In order to reduce simulation errors, the requirements for finite element simulation accuracy are growing, and the corresponding single simulation time increases significantly [15]. In the process of finite element optimization, the finite element model should be continuously optimized according to the simulation results until the optimization target is reached [16]. Therefore, finite element optimization has the disadvantages of a high computational cost, a cumbersome process, low computational efficiency, and difficulty finding the optimal global solution, which is not suitable for the structural optimization of hinge beams.

Modern optimization algorithms have the advantages of low cost, high efficiency, and good optimization effect, which are superior in structural optimization [17,18]. In practical optimization problems, there are often multiple conflicting optimization objectives, and single-objective optimization algorithms cannot optimize multiple objectives simultaneously [19,20]. Li [21] adopted the linear weighting method to transform a multi-objective optimization problem considering energy consumption, stroke, and flow range into a single-objective optimization problem. The throttle groove parameters of the multi-way valve spool were optimized using a genetic algorithm, which resulted in significantly lower energy consumption, a wider speed range, and a 27% increase in effective stroke. However, the selection of the weight coefficients is very subjective and will affect the accuracy of the optimization results. The NSGA-II multi-objective optimization algorithm can prevent the selection of weight coefficients. Wang [22] optimized the atomization nozzle structure using the NSGA-II optimization algorithm, and the optimization results showed that the turbulent kinetic energy and vapor volume fraction were increased by 28.26% and 5.56%, respectively.

Most previous studies on the structural optimization of hinge beams have used finite element optimization methods without considering both safety and economy, resulting in poor and inefficient structural optimization [10,23,24]. This paper investigates the structural optimization for the hinge beam of a cubic press with safety and economy as the optimization objectives. Firstly, the finite element model of a hinge beam is established to analyze its internal stress distribution under rated operating conditions. Secondly, the optimization variables are determined by design insight, the influence of optimization variables on the maximum stress and the total weight is analyzed using the Taguchi method, and its data are provided for the establishment of the objective function. Finally, the entropy-TOPSIS method and the NSGA-II multi-objective algorithm are synthesized to optimize the structure of the hinge beam, obtaining the optimal structural parameters of the hinge beam that take into account safety and economy.

2. Finite Element Simulation

2.1. Finite Element Model Setup

The cubic press is composed of three parts, mechanical, hydraulic, and electrical, which need the interplay of the three to provide a high temperature and high-pressure environment for diamond synthesis. The mechanical structure of the main machine consists of six identical hinge beams arranged in six directions: top, bottom, left, right, front, and back, which are hinged to each other by pins to form a hexahedron structure [25]. As a key component in the loading process of the cubic press, the hinge beam system is subjected to a long-term alternating load with the potential of failure and damage, and it is also the largest and heaviest component.

In this paper, the comprehensive performance of the hinge beam is improved by replacing new materials, adopting new processes, and developing new structures, respectively. Firstly, an improved version of the ductile iron material is adopted. Its yield strength is 1035 MPa, which is 41.8% higher than that of the traditional hinge beam material. Secondly, the forging process is applied. The stiffness and strength of the forged hinge beam are much higher than those of the cast one, which greatly improves the reliability of the press. Finally, a new structure is developed. The new hinge beam does not have a working cylinder and has reinforcement at the bottom. It effectively extends the lifetime of the cubic press and significantly reduces the total weight, thereby increasing corporate profits.

According to the actual working requirements of the hinge beam and the above improvement scheme, the finite element model of the hinge beam is established, as shown in Figure 1. In addition, the finite element model is simplified as follows without affecting the computational accuracy: the rounded corners, chamfers, and threaded hole are ignored.

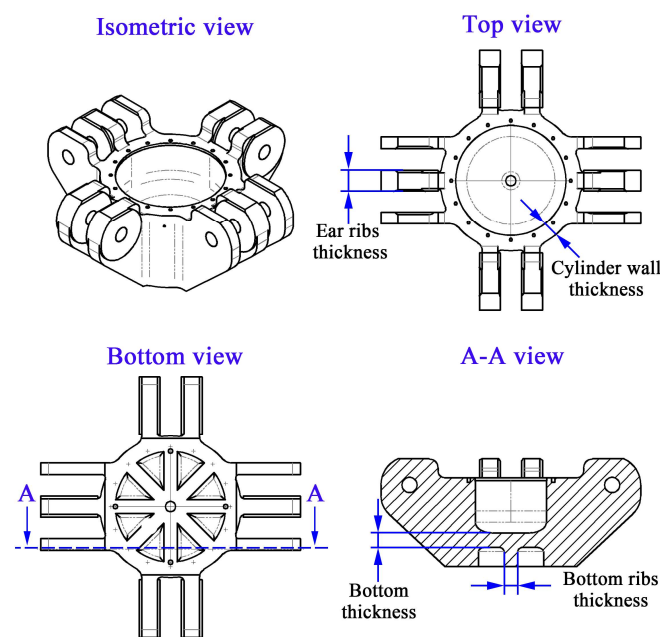


Figure 1. Geometry diagram of hinge beam.

Mesh division is the most important part of the preprocessing for building a finite element model. It needs to be integrated with the specific engineering problem, and the mesh form will directly affect the computational accuracy, computational scale, and convergence [26]. The larger the mesh division, the faster the iteration speed of the finite element simulation, but the simulation results are often unreliable. Conversely, the smaller the mesh division, the more reliable the simulation results are, but it takes a long time. Therefore, both aspects must be taken into account to reduce the mesh number as much as possible while satisfying the computational accuracy.

In order to ensure mesh accuracy, the simulation results are solved by gradually increasing the mesh density. When the simulation results tend to be stable, the mesh accuracy meets the requirements. Figure 2 shows the situation of equivalent stress changing with mesh quantity. It can be observed from the graph that when the mesh quantity reaches 121,859, the equivalent stress mostly stops changing. Therefore, the calculation results can be considered to no longer be dependent on the mesh at this point. The final mesh size is 20 mm, the mesh number is 121,859, the node number is 207,140, and the mesh type is Solid187, which has ten nodes, and each node has three translational degrees of freedom. Solid187 has strong boundary adaptation and displacement flexibility and is suitable for meshing irregular geometry models [27]. Figure 3a shows the finite element meshing model of the hinge beam.

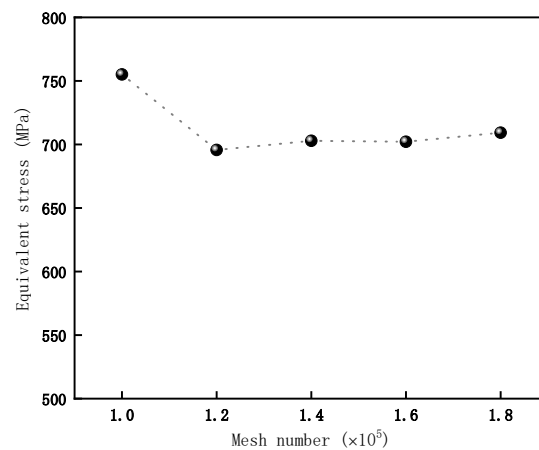


Figure 2. The situation of the equivalent stress changing with the mesh number of finite element.

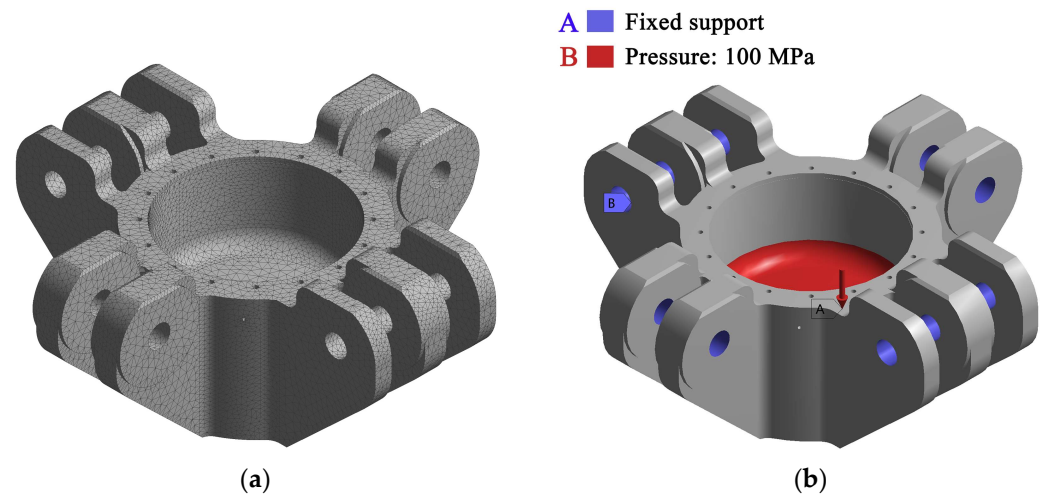


Figure 3. Hinge beam finite element model setup: (a) finite element mesh model; (b) boundary condition.

During the cubic press operation, hydraulic oil flowing from the inlet pushes the piston forward with a rated pressure of 100 MPa. According to Pascal's principle, the oil pressure will be evenly loaded on each surface of the working chamber, so a 100 MPa pressure is applied to the bottom of the hinge beam. Furthermore, the hinge beams are connected to each other by a cylindrical pin, which constrains the motion of the hinge beam, so fixed constraints are applied to the ten cylindrical pin holes. Figure 3b presents the boundary condition setup for the finite element model of the hinge beam.

2.2. Finite Element Results

The allowable stress is $[\sigma_{-1}] = \sigma_s / [n] = 690$ MPa, taking a safety factor of $[n] = 1.5$. Figure 4 shows the equivalent stress diagram of an unoptimized hinge beam under rated conditions. From the diagram, it can be observed that there is stress concentration at the ear's inner edge and oil inlet hole, which is prone to fatigue fracture under repeated external loads [28]. Further observing the stress value color bars, it can be found that the equivalent stress values at either location are non-maximal, indicating that they are not the weakest positions of the hinge beam.

Figure 5 shows the equivalent stress diagram at the bottom of an unoptimized hinge beam under rated conditions. It can be seen that the maximum equivalent stress of the hinge beam is located at the edge of the inlet hole with a value of 695.64 MPa, which is where the hinge beam is most likely to break down. In addition, the oil inlet hole is assembled with the standard oil pipe, and the inlet hole structure needs to be determined

according to the oil pipe, so the inlet hole structure cannot be optimized to reduce the local stress concentration. It can also be noticed that the equivalent stress of the hinge beam is not uniformly distributed, and the equivalent stress of the cylinder wall, ear, and bottom is smaller, which suggests that there is optimization room for the structure and quality of these places.

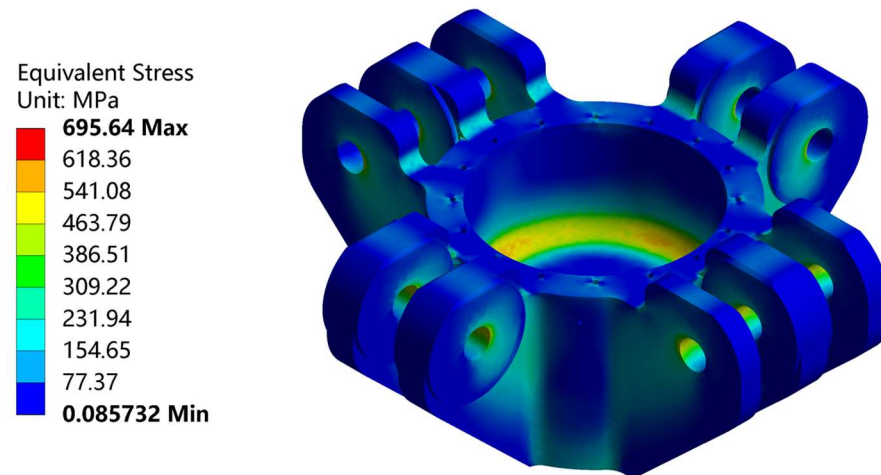


Figure 4. Equivalent stress of an unoptimized hinge beam under rated conditions.

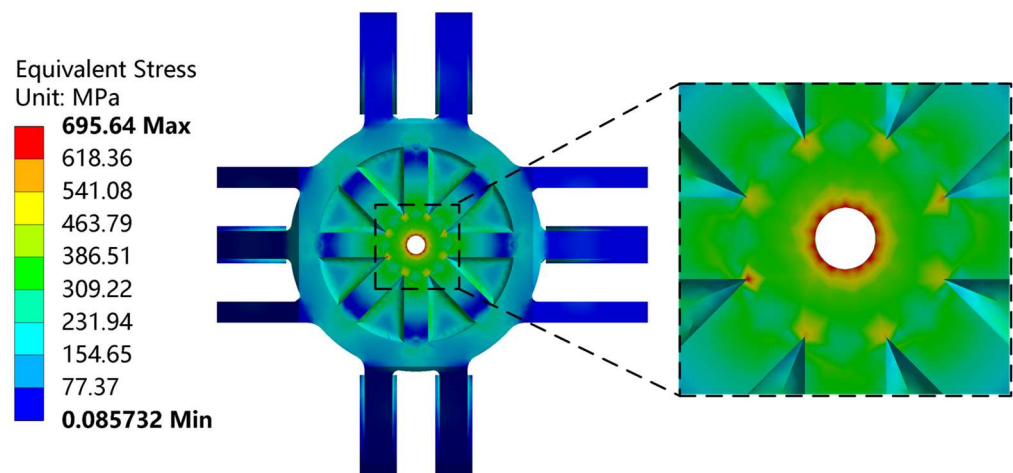


Figure 5. Equivalent stress at the bottom of an unoptimized hinge beam under rated conditions.

3. Taguchi Method

3.1. Influencing Factors

Solidworks Simulation provides the “design insight” analysis tool, which reflects the load distribution on the part body and shows the area where the part can be loaded, guiding structural optimization and improving the part [29]. The structure’s thickness is reduced under a small load, thus greatly improving the structure’s rationality and material utilization.

The design insight of an unoptimized hinge beam is shown in Figure 6. The dark-color represents the part with a higher load, and the light colored represents the part with a lower load. The light-colored material can be selectively removed in the optimization process, thus reducing the overall part while ensuring its strength.

The design of the hinge beam shown in Figure 6 shows that the bottom, ears, and cylinder walls are light-colored, so they are subjected to less load. With the premise of not affecting the working requirements and assembly of the hinge beam, the ear ribs

thickness, cylinder wall thickness, bottom ribs thickness, and bottom thickness can be taken as optimization variables for the lightweight study.

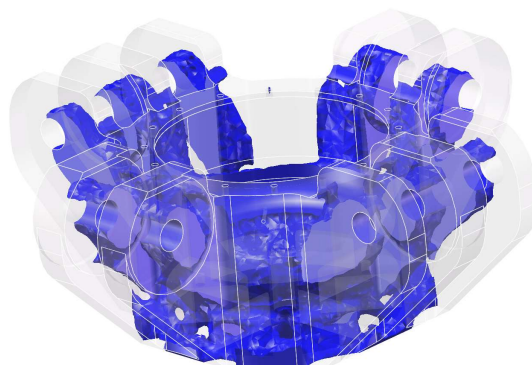


Figure 6. Design insight of an unoptimized hinge beam.

3.2. Taguchi Method Setup

Taguchi method is an effective method to study multi-factor and multi-level problems, requiring only a few representative experiments to reflect the whole experimental situation, which effectively improves the experimental efficiency and reduces the number and cost of tests [30]. In this paper, four important structural parameters of the hinge beam are selected as influencing factors—bottom thickness (A), ear ribs thickness (B), bottom ribs thickness (C), and cylinder wall thickness (D)—and four levels were set for each influencing factor, ignoring the interaction between the influencing factors. The total weight (M) and maximum stress (τ) were taken as the test indexes. According to the data provided by the material supplier, the material strength and processing costs are most appropriate when the thickness is in the range of 105–120 mm. Therefore, the range of each influencing factor is set to 105–120 mm. The Taguchi experimental design for the structural optimization of the hinge beam is shown in Table 1.

Table 1. Taguchi experimental design.

Levels	Influencing Factors			
	A	B	C	D
1	105	105	105	105
2	110	110	110	110
3	115	115	115	115
4	120	120	120	120

3.3. Taguchi Method Results

The simulation results for each scheme are shown in Table 2, and subsequently, the range analysis of the experimental data is performed to further investigate the effects of different structural parameters on the total weight and maximum stress.

The interval analysis method, which is simple and intuitive, is used to obtain the influence weights of each influencing factor on the test indexes. The larger the polar difference the R, the greater the influence of this influencing factor on the test index. Table 3 shows the results for the range analysis of maximum stress, which shows that the order of significance of each influencing factor on maximum stress is $C > D > A > B$. The bottom ribs' thickness has the greatest influence on the maximum stress, followed by the cylinder walls' thickness, while the ear ribs' thickness have the least influence.

Table 4 shows the results for the range analysis of total weight, from which we can see that the order of significance of each influencing factor on total weight is $D > B > C > A$. The cylinder wall thickness has the greatest effect on the total weight, followed by the ear ribs thickness, and then the bottom ribs thickness, and the bottom thickness has the least

effect. From the aforementioned range analysis, it is clear that there is a major difference in the factor significance order on the total mass and maximum stress, indicating that when optimizing one objective, the other objective becomes worse.

Table 2. Taguchi experimental results.

No.	Influencing Factors				Results	
	A	B	C	D	M	σ
1	105	105	105	105	4586.83	710.34
2	105	110	110	110	4678.18	702.58
3	105	115	115	115	4770.84	690.01
4	105	120	120	120	4861.57	658.08
5	110	105	110	115	4716.86	690.42
6	110	110	105	120	4785.54	694.23
7	110	115	120	105	4684.74	681.34
8	110	120	115	110	4752.77	686.57
9	115	105	115	120	4792.65	679.88
10	115	110	120	115	4765.63	672.37
11	115	115	105	110	4711.93	696.82
12	115	120	110	105	4698.33	694.42
13	120	105	120	110	4753.26	661.17
14	120	110	115	105	4663.56	685.41
15	120	115	110	120	4840.01	683.89
16	120	120	105	115	4800.72	687.07

Table 3. Range analysis of maximum stress.

	A	B	C	D
K1	690.253	685.452	697.115	692.877
K2	688.14	688.647	692.827	686.785
K3	685.873	688.015	685.467	684.967
K4	679.385	681.535	668.24	679.02
R	10.868	7.112	28.875	13.857
Ranking		C > D > A > B		

Table 4. Range analysis of total mass.

	A	B	C	D
K1	4724.305	4712.35	4721.205	4658.315
K2	4734.977	4723.228	4733.345	4724.035
K3	4742.135	4751.88	4744.955	4763.513
K4	4764.387	4778.347	4766.3	4819.943
R	40.082	65.997	45.095	161.628
Ranking		D > B > C > A		

4. Multi-Objective Optimization

Multi-objective optimization problems are quite different from single-objective optimization problems. When there is only one objective function, the global maximum or global minimum can be found. Multi-objective optimization is the compromise and coordination of multiple objectives to achieve the best overall objective when solving an optimization problem with multiple objectives [31].

Economic and safety objectives are conflicting goals, where an improvement in one performance leads to a decrease in the other performance. Under the given conditions, it is necessary to achieve a balance between economy and safety. To maximize the benefits and work safely and reliably at the same time, this paper takes the total weight and maximum stress as optimization objectives and makes compromise balance between them to determine the optimal structure of the hinge beam.

The optimization result of the multi-objective optimization problem is a solution set, and these solutions cannot be evaluated as better or worse for the optimization objective, so the corresponding solutions need to be determined according to the actual working conditions. Traditional multi-objective optimization methods such as the weighted summation method, linear programming method, and ϵ -constraint method are ineffective and even fail in the absence of experience. The multi-objective optimization algorithm based on Pareto's dominance principle can avoid the above problems. Figure 7 shows the Pareto dominance theory, which is defined as $\forall x_1, x_2 \in R^N$, if for all $k = 1, \dots, K$, there are $f_k(x_1) \leq f_k(x_2)$, which is called x_1 domination x_2 .

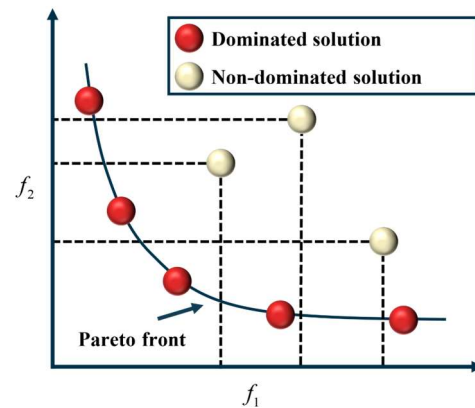


Figure 7. Pareto dominance theory.

The structure optimization process for the hinge beam of a cubic press is given in Figure 8. Firstly, the simulation data of the Taguchi method are processed with the multiple nonlinear regression method to obtain the objective function; secondly, the NSGA-II multi-objective optimization algorithm is applied to coordinate the objective functions and obtain the Pareto-optimal solution set satisfying the constraints. Finally, the Pareto-optimal solution set is evaluated and preferably selected according to the entropy-TOPSIS method to determine the optimal structural solution of the hinge beam.

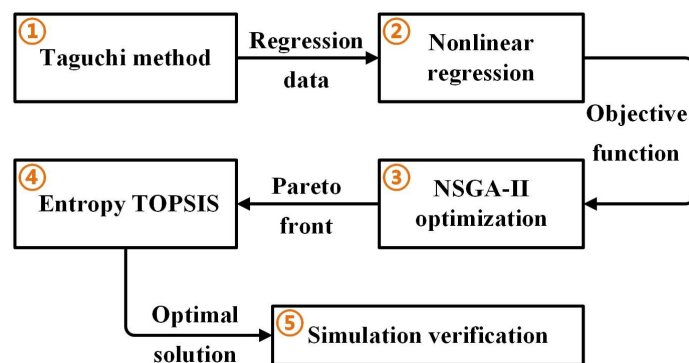


Figure 8. Hinge beam structure optimization process.

4.1. Objective Function

The multiple nonlinear regression method can establish complex relationships between multiple independent variables and one dependent variable, accurately describing the nonlinear relationship that exists between these variables. In this paper, we have applied the multiple nonlinear regression method to process the Taguchi experimental data presented in Table 2. Through this analysis, we have obtained the relationship between key structural parameters and total weight, as well as the relationship between key parameters and maximum stress shown in Equations (1) and (2):

$$M = -2275.6676 + 23.9584x_1 + 65.8153x_2 + 26.1741x_3 - 9.2585x_4 - 0.4086x_1x_2 + 0.0949x_1x_3 + 0.1132x_1x_4 - 0.2538x_2x_3 + 0.1224x_2x_4 - 0.0621x_3x_4 \quad (1)$$

$$\sigma = 1761.3179 - 15.6303x_1 - 0.9384x_2 - 4.9277x_3 + 5.4355x_4 + 0.0667x_1x_2 + 0.0272x_1x_3 + 0.0386x_1x_4 + 0.0189x_2x_3 - 0.078x_2x_4 - 0.0156x_3x_4 \quad (2)$$

where M is the total weight, σ is the maximum stress, x_1 is the bottom thickness, x_2 is the ear ribs' thickness, x_3 is the bottom ribs thickness, and x_4 is cylinder wall thickness.

This paper aims to optimize the bottom thickness x_1 , the ear ribs' thickness x_2 , the bottom ribs' thickness x_3 , and the cylinder walls' thickness x_4 to minimize the total weight and the maximum stress while satisfying the constraints.

$$\begin{aligned} \min & \begin{cases} M(x_1, x_2, x_3, x_4) \\ \tau(x_1, x_2, x_3, x_4) \end{cases} \\ \text{s.t.} & 105 \leq x_1, x_2, x_3, x_4 \leq 120 \end{aligned} \quad (3)$$

4.2. NSGA-II Algorithm

Holland proposed the genetic algorithm (GA) based on Darwinian evolution, which is one of the most widely used multi-objective optimization algorithms, but its weak local search capability easily leads to premature convergence in practical applications. To overcome the shortcomings of GA, Srinivas and Deb [32] combined the advantages of genetic algorithm and Pareto to propose the non-dominated sorting genetic algorithm (NSGA), which improves the search speed and has a strong merit-seeking capability. However, it has high computational complexity and poor population diversity. To solve this problem, Deb [33] introduced fast non-dominated sorting, elite selection strategy, and crowding distance sorting to improve the NSGA algorithm and proposed the NSGA-II algorithm, which has the advantages of fast running speed, excellent robustness, and better convergence of solution sets.

Figure 9 shows the algorithmic principle of NSGA-II. First, initialize the parent population P_t according to the existing parameter range and objective function. Second, perform fast non-dominated sorting and crowding distance calculation for the parent population P_t . Then, generate the new offspring population Q_t using the selection, crossover, and mutation operations. Finally, combine the parent and offspring populations into a new population R_t , perform fast non-dominated sorting and crowding distance calculation for the new population R_t , select the individuals to enter the individuals of the next generation, and so on, until the condition is satisfied.

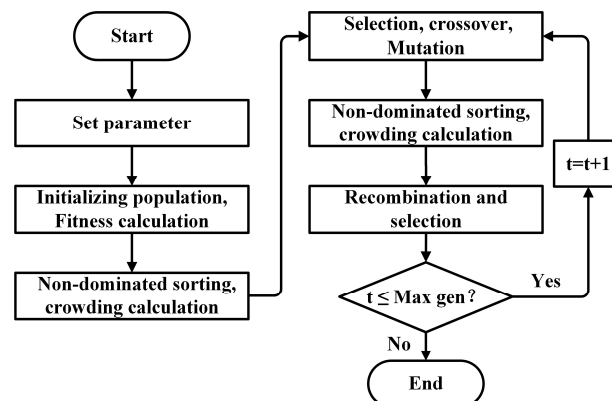


Figure 9. NSGA-II algorithm principle.

The offspring population determination law of the NSGA-II algorithm is given in Figure 10. The individuals with high-dominance rank and big crowding in the new

population R_t are selected to enter the new generation population by using non-dominance sorting and crowding sorting, respectively. The non-dominance sorting principle is shown in Figure 11a, which compares the dominance relationship between different individuals to determine the corresponding dominance rank. The non-dominance layer with the highest dominance rank is called the Pareto front, and the higher the dominance rank is, the higher the possibility of entering the new generation.

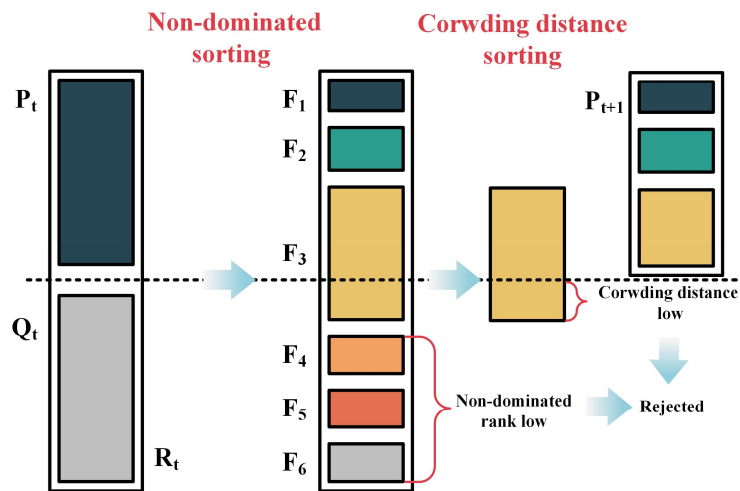


Figure 10. Offspring populations determination law of the NSGA-II algorithm.

The calculation principle of crowding distance is shown in Figure 11b. The crowding distance is used for estimating the surrounding solution density to ensure the uniform distribution of the population in the target space, which in turn ensures the individual diversity of the population. The crowding distance of the i th individual is the sum of the deviations of all objective function values of the $i+1$ th and $i-1$ th individuals, which is calculated as follows:

$$i_{distance} = \sum_{k=1}^m \frac{z_k(k+1) - z_k(k-1)}{z_k^{max} - z_k^{min}}, 2 \leq i \leq n - 1 \tag{4}$$

where m is the number of objective functions, $z_k(i)$ is the k th objective function value corresponding to the i th solution, n is the number of solutions contained in different ranks, and z_k^{max} and z_k^{min} are the maximum and minimum values of the k th objective function set, respectively.

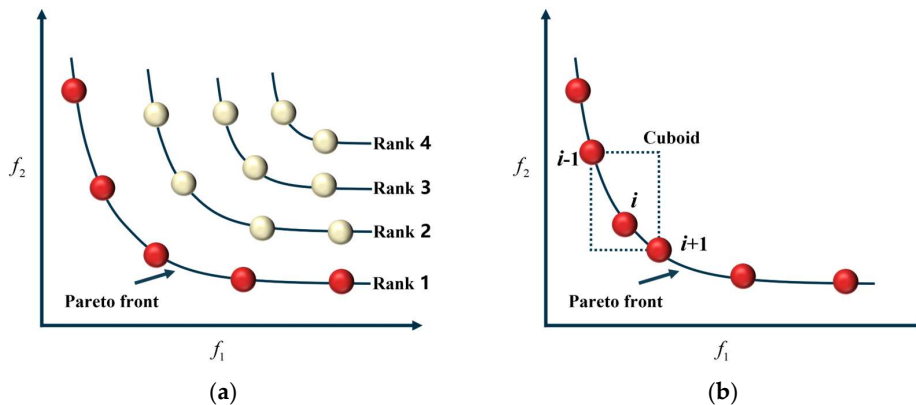


Figure 11. Sorting methods in NSGA-II algorithm: (a) non-dominated sorting; (b) crowding distance sorting.

4.3. Optimization Results

Based on the algorithmic principle described above, numerical simulations are carried out by utilizing MATLAB. We referred to the parameter range of the NSGA-II algorithm and adjusted its parameters based on the characteristics of our research target. The specific parameters are as follows: the population size is 50; the maximum iteration number is 50; the crossover probability and the variance probability are 0.8 and 0.05, respectively, and the optimization objectives are the total weight and the maximum stress. Figure 12 presents the Pareto front for multi-objective structural optimization of the hinge beam. As can be seen, the optimal solution set of the Pareto front is uniformly distributed along one curve, where each solution has at least one objective function value better than the others. As the maximum stress decreases, the total weight tends to rise, and there is a mutually exclusive relationship between them.

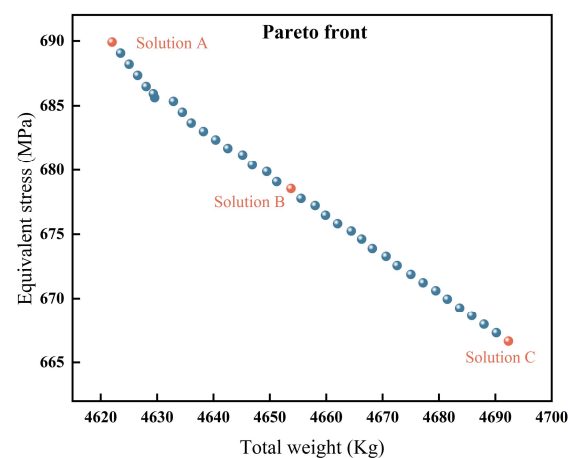


Figure 12. Pareto front for multi-objective structural optimization of hinge beam.

In the Pareto front, there is no clear superiority or inferiority between any two solutions. Researchers usually determine the solutions based on the target tendency and manual experience. The optimal solutions based on the three different target preferences in Figure 12 are given in Table 5. As can be seen in the table, Solution A has a tendency to minimize the total weight, the total weight is 4622.019 kg, and the maximum stress is 689.91 MPa under the structural parameters of Solution A. Solution B comprehensive consideration of total weight and maximum stress, the total weight is 4653.744 kg, and the maximum stress is 678.55 MPa under the structural parameters of Solution B. Solution C tends to minimize the maximum stress, the total weight is 4692.336 kg, and the maximum stress is 666.64 MPa under the structural parameters of solution C.

Table 5. Optimal solutions based on manual experience.

Solution	Structural Parameters				Results	
	Bottom Thickness (mm)	Ear Ribs Thickness (mm)	Bottom Ribs Thickness (mm)	Cylinder Wall Thickness (mm)	Total Weight (kg)	Equivalent Stress (MPa)
Solution A	105.5	105	117.5	105	4622.019	689.91
Solution B	111.5	105	119.5	105	4653.744	678.55
Solution C	120	105	120	105	4692.336	666.64

All the above-mentioned solutions have their own advantages, and the solutions are generally determined according to the actual needs. Economically, option A is the optimal choice; when considering the safety of equipment operation, the equipment is most reliable under the structural parameters of option C. However, both solutions, A and C, are extreme

values, where one goal is optimal while the other goal performs the worst. Considering this problem, scheme B compromises to balance the total weight and maximum stress and to reduce the overall cost as much as possible while ensuring safety. However, the above schemes are determined based on manual experience, and it is not analyzed quantitatively or qualitatively whether they meet the requirements.

4.4. Entropy-TOPSIS Method

TOPSIS is a decision-making method based on ideal and negative ideal solutions, and it is widely used to determine the Pareto-optimal solution [34]. The ideal and negative ideal solutions are virtual optimal and worst solutions, which represent the optimal and worst values in each objective function, respectively. However, the TOPSIS method achieves artificial subjective interference by using subjective weights in constructing the weighted normalization matrix.

Therefore, the entropy weighting method can objectively determine the weight coefficients and thus more realistically reflect the importance of each factor [35]. Combining the entropy weighting method with the TOPSIS method to determine the optimal solution of the Pareto front can effectively avoid manual interference. The entropy weight calculation process is as follows:

- (1) Constructing and normalizing the decision matrix

Assuming that there are n evaluation objects and m evaluation indicators, a decision matrix can be constructed as

$$X = \begin{bmatrix} x_{11} & x_{12} & \cdots & x_{1m} \\ x_{21} & x_{22} & \cdots & x_{2m} \\ \vdots & \vdots & \ddots & \vdots \\ x_{n1} & x_{n2} & \cdots & x_{nm} \end{bmatrix} \quad (5)$$

Let the normalized matrix be Y , where the elements are denoted as follows:

$$y_{ij} = \frac{x_{ij}}{\sqrt{\sum_{i=1}^n x_{ij}^2}} \quad (6)$$

- (2) Calculate the information entropy value, probability matrix, and entropy weight as follows:

$$e_j = -\frac{1}{\ln n} \sum_{i=1}^n p_{ij} \ln(p_{ij}), \quad (j = 1, 2, L, m) \quad (7)$$

where n is the number of evaluation indexes and p_{ij} is the element of probability matrix P :

$$p_{ij} = y_{ij} / \sum_{i=1}^n y_{ij} \quad (8)$$

The corresponding entropy weight of each evaluation object is obtained by the information entropy value:

$$W_j = \frac{1 - e_j}{\sum_{j=1}^m (1 - e_j)} \quad (9)$$

- (3) Calculate the Euclidean distance of each evaluation index relative to the ideal and the negative ideal.

The matrix forward normalization methods for extremely large types and extremely small types are

$$A_{ij} = \frac{y_{ij} - \min_j(y_{ij})}{\max_j(y_{ij}) - \min_j(y_{ij})} \tag{10}$$

$$A_{ij} = \frac{\max_j(y_{ij}) - y_{ij}}{\max_j(y_{ij}) - \min_j(y_{ij})} \tag{11}$$

The weighted normalized matrix is constructed as

$$B = (b_{ij})_{n \times m} = (A_{ij}W_j)_{n \times m} \tag{12}$$

The Euclidean distance is calculated as

$$D_i^+ = \sqrt{\sum_{j=0}^m (b_{ij} - b_i^+)^2} \tag{13}$$

$$D_i^- = \sqrt{\sum_{j=0}^m (b_{ij} - b_i^-)^2} \tag{14}$$

where $b_i^+ = \max\{b_{1j}, b_{2j}, \dots, b_{nj}\}$, $b_i^- = \min\{b_{1j}, b_{2j}, \dots, b_{nj}\}$ are the ideal and negative ideal solutions, respectively.

(4) The relative closeness is determined as

$$C_i = \frac{D_i^+}{D_i^+ + D_i^-} \tag{15}$$

The relative closeness of each solution is calculated according to Equation (15), and C_i is the relative closeness of the i th solution, and the larger its value, the better the solution is.

4.5. Optimal Solution and Validation

The entropy weight of total weight and maximum stress is calculated according to Equations (5)–(9), which is 0.5198 and 0.4802, respectively. In the optimization of the hinge beam structure, the total weight entropy value is greater and occupies a more important position. Table 6 shows the optimal solution selected from the Pareto front using the entropy–TOPSIS method. Compared to the initial solution, the total weight and maximum stress are reduced by 199.121 kg and 11.97 MPa, respectively, with a reduction of 4.12% and 1.72%. This optimal solution not only ensures the equipment working safety but also greatly reduces its manufacturing cost.

Table 6. Optimal solution of the hinge beam structure based on the entropy–TOPSIS method.

Solution	Structural Parameters				Results	
	Bottom Thickness (mm)	Ear Ribs Thickness (mm)	Bottom Ribs Thickness (mm)	Cylinder Wall Thickness (mm)	Total Weight (kg)	Equivalent Stress (MPa)
Initial solution	110	120	105	120	4835.175	695.64
Optimal solution	107	105	120	105	4636.054	683.67
Decrease					4.12%	1.72%

To validate the optimization results of the algorithm, a numerical simulation of the hinge beam is performed using the optimal structural parameters, and the results are

presented in Figure 13. The simulation results show that the maximum stress and total weight of the optimal structural parameters are 681.79 Mpa and 4625.874 kg, respectively. Comparison with the algorithm's optimization results for the maximum stress and total weight of the optimal structural parameters in Table 6 reveals that the simulation errors for total weight and maximum stress are 0.22% and 0.27%, respectively. The simulation errors are extremely small, which indicates that the structural optimization method of the hinge beam with the combined entropy–TOPSIS method and NSGA-II multi-objective algorithm has high reliability.

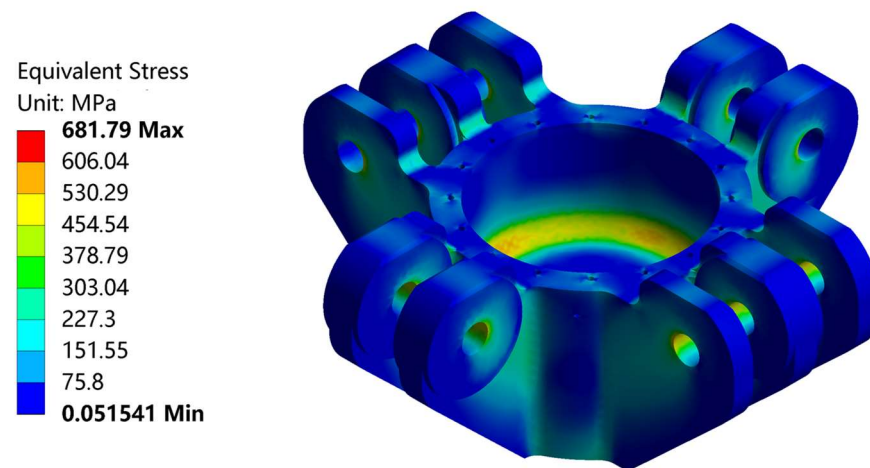


Figure 13. Equivalent stress of an optimized hinge beam under rated conditions.

5. Conclusions

The traditional structural optimization method relies on finite element verification, which requires a large number of simulation attempts, and then iteratively optimizes the direction and parameters of optimization through analysis of simulation results. The structural optimization method proposed in this paper can effectively improve the optimization efficiency and can handle different optimization objectives to find a better balance and finally achieve better performance and lower cost. The main findings are summarized as follows:

- (1) The FEM results show that the stress distribution of the hinge beam is not uniform under the rated working condition, which has a serious stress concentration. The maximum equivalent stress of the hinge beam is located at the inlet hole edge with a value of 695.64 MPa.
- (2) The range analysis results show that the bottom ribs' thickness has the greatest effect on the maximum stress, while the cylinder walls' thickness has the greatest effect on the total weight. The large differences in factor significance order for maximum stress and total weight indicate safety and economy as conflicting optimization objectives.
- (3) Based on the entropy–TOPSIS method and the NSGA-II multi-objective optimization algorithm, the following optimal structural parameters of the hinge beam are obtained: bottom thickness 107 mm, ear ribs thickness 105 mm, bottom ribs thickness 120 mm, and cylinder wall thickness 105 mm. The total weight and maximum stress are reduced by 199.121 kg and 11.97 MPa, respectively, with a reduction of 4.12% and 1.72%.
- (4) Numerical simulations of the hinge beam are carried out under the optimal structural parameters. The simulation results of the maximum stress and total weight are 681.79 MPa and 4625.874 kg, respectively, and the algorithm optimization results for the maximum stress and total weight are 683.67 MPa and 4636.054 kg, respectively. Upon comparing the algorithm optimization and simulation results, we found that the simulation error is 0.22% for total weight and 0.27% for maximum stress. This indicates that the hinge beam structure optimization method adopted in this paper is

accurate and reliable, which effectively shortens the development cycle of the new hinge beam and reduces the cubic press total cost.

Author Contributions: Conceptualization, J.S. and T.L.; methodology, J.S. and J.J.; software, J.S.; validation, J.S.; writing—original draft preparation, J.S.; writing—review and editing, J.S. and X.S.; funding acquisition, X.S. All authors have read and agreed to the published version of the manuscript.

Funding: This research was funded by the Strength Calculation and Optimization Analysis of Hinge Sleeve of Cubic equipment, grant number RH2100002691.

Institutional Review Board Statement: Not applicable.

Informed Consent Statement: Not applicable.

Data Availability Statement: Not applicable.

Conflicts of Interest: The authors declare no conflict of interest.

References

1. Gan, J.; Gao, H.; Wen, S.; Zhou, Y.; Tan, S.; Duan, L. Simulation, forming process and mechanical property of Cu-Sn-Ti/diamond composites fabricated by selective laser melting. *Int. J. Refract. Met. Hard Mater.* **2020**, *87*, 105144. [\[CrossRef\]](#)
2. Fu, S.; Yang, H.; Sun, S.; Zhang, M.; Liu, Y.; Zhang, Y.; Jiang, Z.; Pan, L. Investigation on the surface roughness modeling and analysis for ultra-precision diamond turning processes constrained by the complex multisource factors. Proceedings of the Institution of Mechanical Engineers. *J. Eng. Manuf. Part B* **2022**, *236*, 1295–1304. [\[CrossRef\]](#)
3. Yang, Y.; Mimouni, M.; Trinh, T.; Sorkin, N.; Cohen, E.; Santaella, G.; Rootman, D.S.; Chan, C.C.; Slomovic, A.R. Phototherapeutic keratectomy versus epithelial debridement combined with anterior stromal puncture or diamond burr for recurrent corneal erosions. *Can. J. Ophthalmol.* **2022**. [\[CrossRef\]](#) [\[PubMed\]](#)
4. Zhu, P.; Wang, P.; Shao, P.; Lin, X.; Xiu, Z.; Zhang, Q.; Kobayashi, E.; Wu, G. Research progress in interface modification and thermal conduction behavior of diamond/metal composites. *Int. J. Miner. Metall. Mater.* **2022**, *29*, 200–211. [\[CrossRef\]](#)
5. Liu, F.; Zhang, D.Z.; Zhang, P.; Zhao, M.; Jafar, S. Mechanical Properties of Optimized Diamond Lattice Structure for Bone Scaffolds Fabricated via Selective Laser Melting. *Materials* **2018**, *11*, 374. [\[CrossRef\]](#)
6. Jiang, X.; Deng, L. Multiphysics coupled plasma simulation of MPCVD diamond single crystal growth. In Proceedings of the International Conference on Computational Modeling, Simulation, and Data Analysis SPIE, Sanya, China, 3–5 December 2021.
7. Vermeeren, V.; Wenmackers, S.; Wagner, P.; Michiels, L. DNA Sensors with Diamond as a Promising Alternative Transducer Material. *Sensors* **2009**, *9*, 5600–5636. [\[CrossRef\]](#)
8. Diggle, P.L.; D’Haenens-Johansson, U.F.S.; Green, B.L.; Welbourn, C.M.; Tran Thi, T.N.; Katrusha, A.; Wang, W.; Newton, M.E. Decoration of growth sector boundaries with nitrogen vacancy centers in as-grown single crystal high-pressure high-temperature synthetic diamond. *Phys. Rev. Mater.* **2020**, *4*, 093402. [\[CrossRef\]](#)
9. Yang, X.; Deng, F. Synthesis and characterisation of $\Phi 62$ mm polycrystalline diamond compact. *Diamond Relat. Mater.* **2019**, *100*, 107594. [\[CrossRef\]](#)
10. Sun, X.; Qi, W.Z.; Zhao, H.; Li, H.X. Study on Fatigue of Hinge Sleeve of Cubic Press based on ANSYS. *Appl. Mech. Mater.* **2014**, *457*, 585–588. [\[CrossRef\]](#)
11. Wu, W.-H.; Young, W.-B. Structural Analysis and Design of the Composite Wind Turbine Blade. *Appl. Compos. Mater.* **2012**, *19*, 247–257. [\[CrossRef\]](#)
12. Guo, Z.; Li, H.; Gu, C. Finite element analysis and structural optimization of V-shaped seal ring based on ANSYS Workbench. *J. Phys. Conf. Ser.* **2022**, *2383*, 012106. [\[CrossRef\]](#)
13. Liu, C.; Wei, X.; Yi, Z.; Li, Z.; Zhu, C.; Ma, Z. Strength Analysis and Structure Optimization of the Crankshaft of an Opposed-Power Reciprocating Pump. *Machines* **2023**, *11*, 123. [\[CrossRef\]](#)
14. Ma, L.; Lu, B.; Yuan, Y.; Zhang, Y. The stress analysis and tests on the hinge beam of the diamond synthesis cubic press. In Proceedings of the 2016 3rd International Conference on Mechanics and Mechatronics Research (ICMMR 2016), Chongqing, China, 15–17 June 2016.
15. Guan, A.; Zhou, S.; Gu, W.; Liu, Z.; Liu, H. A novel dynamic simulation approach for Gas-Heat-Electric coupled system. *Appl. Energy* **2022**, *315*, 118999. [\[CrossRef\]](#)
16. Wang, Y.; Zhao, J.; Zhao, R. Shape Parameterization Optimization of Thermocouples Used in Aeroengines. *Aerospace* **2023**, *10*, 202. [\[CrossRef\]](#)
17. Saka, M.P.; Hasançebi, O.; Geem, Z.W. Metaheuristics in structural optimization and discussions on harmony search algorithm. *Swarm Evol. Comput.* **2016**, *28*, 88–97. [\[CrossRef\]](#)
18. Tan, W.; Chen, Z.; Li, Z.; Yan, H. Thermal-Fluid-Solid Coupling Simulation and Oil Groove Structure Optimization of Wet Friction Clutch for High-Speed Helicopter. *Machines* **2023**, *11*, 296. [\[CrossRef\]](#)
19. Song, Z.; Li, J.; Han, X.; Xu, L.; Lu, L.; Ouyang, M.; Hofmann, H. Multi-objective optimization of a semi-active battery/supercapacitor energy storage system for electric vehicles. *Appl. Energy* **2014**, *135*, 212–224. [\[CrossRef\]](#)

20. Hou, J.; Li, S.; Pan, W.; Yang, L. Co-Simulation Modeling and Multi-Objective Optimization of Dynamic Characteristics of Flow Balancing Valve. *Machines* **2023**, *11*, 337. [[CrossRef](#)]
21. Li, C.; Liu, X.; Wang, X.; Chen, J.; Wang, Y. Optimization of Multi-Way Valve Structure in Digital Hydraulic System of Loader. *Energies* **2021**, *14*, 700. [[CrossRef](#)]
22. Wang, Z.; Sun, X.; Chen, S. Multi-objective parameters optimization design of self-excited oscillation pulsed atomizing nozzle. *J. Braz. Soc. Mech. Sci. Eng.* **2019**, *41*, 510. [[CrossRef](#)]
23. Sun, X.; Shi, J.X.; Zhong, Z.X.; Zhao, H. Study on architecture of measurement of multi-points strain of hinge sleeve of cubic press under super-high pressure. *Appl. Mech. Mater.* **2014**, *596*, 472–475. [[CrossRef](#)]
24. Li, R.; Xu, B.; Zhang, Q.; Gu, X.; Zheng, G.; Ma, H.; Jia, X. Finite-element analysis on pressure transfer mechanism in large-volume cubic press. *High Press. Res.* **2016**, *36*, 575–584. [[CrossRef](#)]
25. Song, G.; Ma, D.; Zhou, X.; Wang, L.; Wei, Z.; Xu, C.; Wang, W.; Wang, L.; Zhao, Y.; Wang, S. Operation of large-volume cubic press above 8 GPa and 2500 °C with a centimeter-sized cell volume using an optimized hybrid assembly. *High Press. Res.* **2021**, *41*, 132–141. [[CrossRef](#)]
26. Wang, M.; Ma, Y.; Liu, F. A novel virtual cutting method for deformable objects using high-order elements combined with mesh optimisation. *Int. J. Med. Robot. Comput. Assist. Surg.* **2022**, *18*, e2423. [[CrossRef](#)] [[PubMed](#)]
27. Revanasiddesh, B.V.; Taj, A.P.; Kumar, N.S.N.; Suresh, B.S. Extraction of modal parameters of CNC lathe bed using finite element and experimental method. *Mater. Today Proc.* **2020**, *24*, 398–405. [[CrossRef](#)]
28. Danicic, D.; Sedmak, S.; Ignjatovic, D.; Mitrovic, S. Bucket Wheel Excavator Damage by Fatigue Fracture—Case Study. *Procedia Mater. Sci.* **2014**, *3*, 1723–1728. [[CrossRef](#)]
29. du Plessis, A.; Broeckhoven, C.; Yadroitsava, I.; Yadroitsev, I.; Hands, C.H.; Kunju, R.; Bhate, D. Beautiful and Functional: A Review of Biomimetic Design in Additive Manufacturing. *Addit. Manuf.* **2019**, *27*, 408–427. [[CrossRef](#)]
30. Mojaver, P.; Khalilarya, S.; Chitsaz, A.; Assadi, M. Multi-objective optimization of a power generation system based SOFC using Taguchi/AHP/TOPSIS triple method. *Sustain. Energy Technol. Assess.* **2020**, *38*, 100674. [[CrossRef](#)]
31. Kitayama, S.; Yamazaki, K. Compromise point incorporating trade-off ratio in multi-objective optimization. *Appl. Soft Comput.* **2012**, *12*, 1959–1964. [[CrossRef](#)]
32. Srinivas, N.; Deb, K. Multiobjective Optimization Using Nondominated Sorting in Genetic Algorithms. *Evol. Comput.* **1994**, *2*, 221–248. [[CrossRef](#)]
33. Deb, K.; Pratap, A.; Agarwal, S.; Meyarivan, T. A fast and elitist multiobjective genetic algorithm: NSGA-II. *IEEE Trans. Evol. Comput.* **2002**, *6*, 182–197. [[CrossRef](#)]
34. Méndez, M.; Frutos, M.; Miguel, F.; Aguasca-Colomo, R. TOPSIS Decision on Approximate Pareto Fronts by Using Evolutionary Algorithms: Application to an Engineering Design Problem. *Mathematics* **2020**, *8*, 2072. [[CrossRef](#)]
35. Zhu, Y.; Tian, D.; Yan, F. Effectiveness of Entropy Weight Method in Decision-Making. *Math. Probl. Eng.* **2020**, *2020*, 3564835. [[CrossRef](#)]

Disclaimer/Publisher’s Note: The statements, opinions and data contained in all publications are solely those of the individual author(s) and contributor(s) and not of MDPI and/or the editor(s). MDPI and/or the editor(s) disclaim responsibility for any injury to people or property resulting from any ideas, methods, instructions or products referred to in the content.